EUROPEAN LABORATORY FOR PARTICLE PHYSICS

NA60 status report

The NA60 Collaboration

Abstract

Several experiments at the CERN SPS have measured lepton pair production in nuclear collisions over more than 15 years. The absence of significant reinteractions with the hadronic environment makes dileptons very attractive to study the early stages of the collision, when thermal dileptons from a deconfined phase are possibly emitted. Furthermore, the vector mesons produced in the collisions (ρ, ω, ϕ, and J/ψ) can be detected in a clean way through their leptonic decay. While a number of exciting results were obtained after the first round of investigations, several points deserved a more detailed investigation. NA60 has been specifically designed with the idea to perform further high precision measurements on (i) the properties of the ρ meson in the strongly interacting dense medium created in a heavy ion collision, (ii) the unambiguous determination of the open charm yield and the quantitative assessment of the production of thermal radiation in the intermediate mass region, and (iii) the study of the J/ψ suppression in a collision system other than Pb-Pb in an attempt to shed light on the mechanisms driving the suppression.

The heavy ion physics program of the experiment has been accomplished in a single data taking period during 2003 using a 158 AGeV/c indium beam. In addition, a second data taking period in 2004 was devoted to proton physics with 158 and 400 GeV/c proton beams. This report is mostly focused on all the physics results that have been obtained so far from the analysis of the large, high quality data sample collected with the indium beam. The three goals defined above are almost reached with (i) the first measurement of the ρ spectral function, showing strong broadening, but essentially no shift in mass, (ii) the finding that charm is not enhanced, attributing all the observed enhanced pair production beyond charm and Drell-Yan to a prompt source (maybe thermal radiation), (iii) the observation of anomalous J/ψ suppression beyond nuclear absorption, with an onset at about 80 participant nucleons. Further results have been obtained on the ϕ and, for the first time, on the elliptic flow of the J/ψ.

The analysis of the proton data is in progress. A short overview of the present status is given in the last part of this report.

1 Experimental set-up and data reconstruction for In-In

The NA60 apparatus and its new vertex tracker have been already described in detail in previous SPSC memoranda and in [1, 2]. Here we briefly recall the detector concept and consider those points in the data reconstruction which are relevant for the discussion of the physics results.

The heart of the NA60 apparatus is the muon spectrometer inherited from NA50. This spectrometer is placed after a hadron absorber, which stops most of the hadrons before they reach the trigger hodoscopes and the tracking chambers. A radiation hard silicon vertex tracker embedded in a 2.5 T dipole magnetic field is placed before the hadron absorber. It reconstructs all charged particle tracks without the problem of the multiple scattering and energy fluctuations which are introduced by the absorber. Tracks are reconstructed in the rapidity window $3.0 < y < 4.3$ (in more detail, the rapidity coverage is $3.3 < y < 4.3$ for the ρ and $3 < y < 4$ for the J/ψ). The resolution for the determination of the vertex position is $10 - 20$ μm in the transverse coordinates and ~ 200 μm along the beam axis.

The data were collected with a 158 AGeV/c indium beam incident on a segmented indium target of seven disks with a total 18% (In-In) interaction length. At an average beam intensity of $5 \cdot 10^7$ ions per 5s burst, about $3 \cdot 10^{12}$ ions were delivered to the experiment, and a total of 230 million dimuon triggers were recorded on tape. Data were taken with two different setups for the muon spectrometer magnet: a low current setup (4000 A), optimized to study the low and intermediate dimuon mass regions, and a high current setup (6500 A), optimized to study the J/ψ.

In order to identify the muons in the vertex region, the tracks reconstructed in the muon spectrometer are extrapolated back to the target region and matched to the tracks reconstructed in the vertex tracker. This is done comparing both angles and curvatures. Once identified, the muons are refitted using the joint information of the muon spectrometer and of the vertex detector. We will refer to these tracks as "matched muons". In this way the mass resolution at the ϕ peak decreases from ~ 80 MeV, when using only the muon spectrometer, to 23 MeV, when using also the information from the vertex detector, independent of centrality. Furthermore, because of the dipole field in the target region, there is also acceptance for low p_T and low mass dimuons as shown in fig. 1. This presents a strong improvement with respect to all previous dimuon experiments.

The matched dimuon data sample is affected by two sources of background: the combinatorial background and the fake matches. The former is the contribution of uncorrelated muon pairs arising from the decay of pions and kaons. The latter is due to the fact that the matching procedure can associate a muon to a wrong track in the vertex tracker. When this happens, the kinematics of the matched muon is highly degraded.

The combinatorial background is subtracted using an event mixing technique: two muons from different events are randomly paired to build a dimuon sample, which
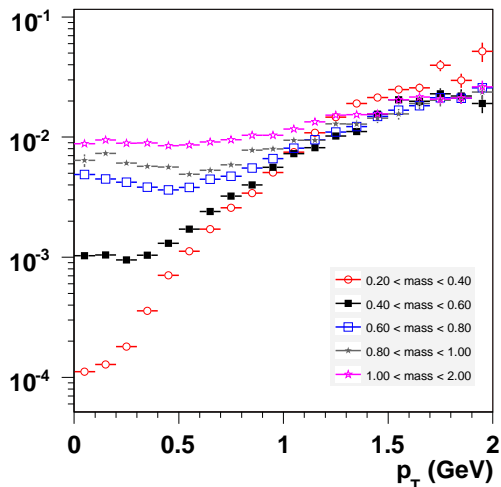
Figure 1: Acceptance relative to 4π as a function of p_T for different dimuon mass intervals.

is uncorrelated by construction. This technique automatically takes into account all experimental details, provided the muons are weighted with the correct occupancy probabilities as extracted from the data [3, 4]. The NA60 apparatus not only triggers on opposite sign pairs ($\mu^+\mu^-$) but also on like-sign pairs ($\mu^+\mu^+$ and $\mu^-\mu^-$) which contain only uncorrelated muons so that the real and mixed spectra for the like-sign pairs should be identical. This fact is used to assess the quality of the estimated combinatorial background. The accuracy is found to be of the order of 1% over the full dimuon mass range [3, 4].

Fake matches, on the other hand, can be estimated in two different ways. The first approach is an overlay Monte Carlo technique, where a Monte Carlo dimuon is reconstructed on top of a real event (in the vertex telescope), allowing to calculate the probability to get a fake match. The second method is an event mixing method, which extracts the probability distributions of fake matches from the data alone. The basic idea is to match the tracks in the muon spectrometer from one event to vertex tracks of a different event [3, 4]. All the matches obtained in this way are fake by construction. This technique is more complicated but more rigorous. The agreement between the two methods is within 5% for low dimuon masses (below the ϕ) and even better at higher masses. This is taken as an estimate of the systematic error in the fake background subtraction.

The experiment can measure the collision centrality either through the charged particle multiplicity as measured by the vertex tracker, or through the energy of the spectator nucleons as measured by a zero degree calorimeter (ZDC).

2

2 The low mass region: the ρ spectral function

Thermal dilepton production in the mass region < 1 GeV/c^2 is largely mediated by the light vector mesons ρ, ω and ϕ. Among these, the $\rho(770)$ is the most important, due to its strong coupling to the $\pi\pi$ channel and its short lifetime of only 1.3 fm/c, much shorter than the lifetime of the fireball. In-medium changes of both its width and mass were originally suggested as precursor signatures of the chiral transition [5]. Previous measurements of electron pair production performed by CERES/NA45 [6, 7, 8] found, in nuclear collisions, an excess of the dilepton yield above the expected yields of neutral mesons, by a factor 2-3 for masses above 0.2 GeV/c^2. This was attributed to direct thermal radiation from the fireball, dominated by pion annihilation $\pi^+\pi^- \to \rho \to \ell^+\ell^-$ with a strongly modified intermediate ρ.

The new NA60 measurement takes advantage of a much larger statistics and improved mass resolution [9, 10, 11, 12]. This has made it possible to assess for the first time in a quantitative way the character of the in-medium changes of the ρ. Fig. 2 shows the opposite-sign, background and signal dimuon mass spectra, integrated over all collision centralities. After subtracting the combinatorial background and the signal fake matches, the resulting net spectrum contains about 360 000 muon pairs in the range from threshold up to 2 GeV/c^2, roughly 50% of the total available statistics. The average charged-particle multiplicity density measured by the vertex tracker is $dN_{ch}/d\eta = 120$, and the average signal-to-background is 1/7. For the first time in nuclear collisions, the vector mesons ω and ϕ are completely resolved in the dilepton channel; even the $\eta \to \mu\mu$ decay is seen. The mass resolution at the ω is 20 MeV/c^2. The further analysis is performed in four classes of collision centrality defined through the charged-particle multiplicity density: peripheral (4–30), semiperipheral (30–110), semicentral (110–170), central (170–240). The signal-to-background ratios associated the individual classes are 2, 1/3, 1/8, and 1/11, respectively.

The peripheral data can be described by the expected electromagnetic decays of the neutral mesons, namely the two-body decays of the η, ρ, ω, and ϕ resonances and the Dalitz decays of the η, η' and ω (the so-called hadron decay cocktail). The cross section ratios η/ω and ϕ/ω calculated in different transverse momentum windows and extrapolated to full phase space are independent of the transverse momentum window within 10%. This indicates that the acceptance corrections vs p_T are correct on the level of 10% even in the low mass and low p_T region.

For more central events, a fit procedure is not possible because of the presence of an excess whose characteristics are not known a priori. However, the high quality of the data has made possible a new procedure, as illustrated in fig. 3 (left). The excess is isolated by subtracting from the data the cocktail, without the ρ. The cocktail is fixed separately for the main sources and in each centrality bin by a "conservative" approach. The yields of the narrow vector mesons ω and ϕ are fixed in such a way to get a smooth underlying continuum after subtraction. For the η, an upper limit is defined by "saturating" the measured data in the region close to 0.2 GeV/c^2. Fig. 3 (right) shows the excess spectra for the 4 multiplicity bins resulting from the
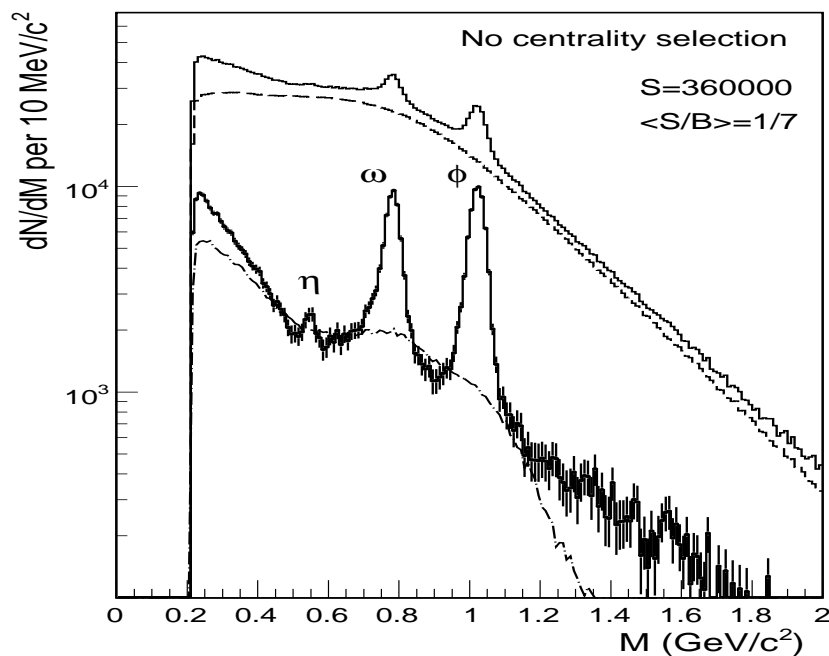
Figure 2: Mass spectra of opposite sign dimuons (upper histogram), combinatorial background (dashed), signal fake matches (dashed-dotted), and resulting signal (histogram with error bars)

subtraction of this "conservative" hadron decay cocktail. The qualitative features of the spectra are striking: a peaked structure is seen in all cases, remaining essentially centered around the position of the nominal ρ pole, but strongly broadening with an increasing yield as a function of centrality.

A quantitative analysis of the evolution of the shape of the excess mass spectra as a function of centrality was performed using a finer subdivision into 12 centrality bins [11]. Data were divided into three mass windows: one central window (C) with $0.64 < M < 0.84$ GeV/c^2 and two side windows L (left) and R (right) of equal size as the central. Measuring the yields in these windows, a peak yield $C - (L + R)/2$ and a continuum yield $3(L + R)/2$ can be determined and compared to the cocktail ρ. Fig 4 (left panel) shows the ratios peak/ρ, continuum/ρ and peak/continuum. The right panel of fig. 4 shows the RMS of the total mass interval $0.44 < M < 1.04$ GeV/c^2. The ratio peak/ρ decreases from the most peripheral to the most central bin by almost a factor of 2, ruling out the naive view that the shape can be simply explained by the cocktail ρ residing on a broad continuum, independent of centrality. The centrality dependences of all variables are consistent in the two plots, including some change in slope beyond $dN_{ch}/dy=100$.

The qualitative features of the excess mass spectra shown in the previous figures are consistent with the interpretation as direct thermal radiation from the fireball,
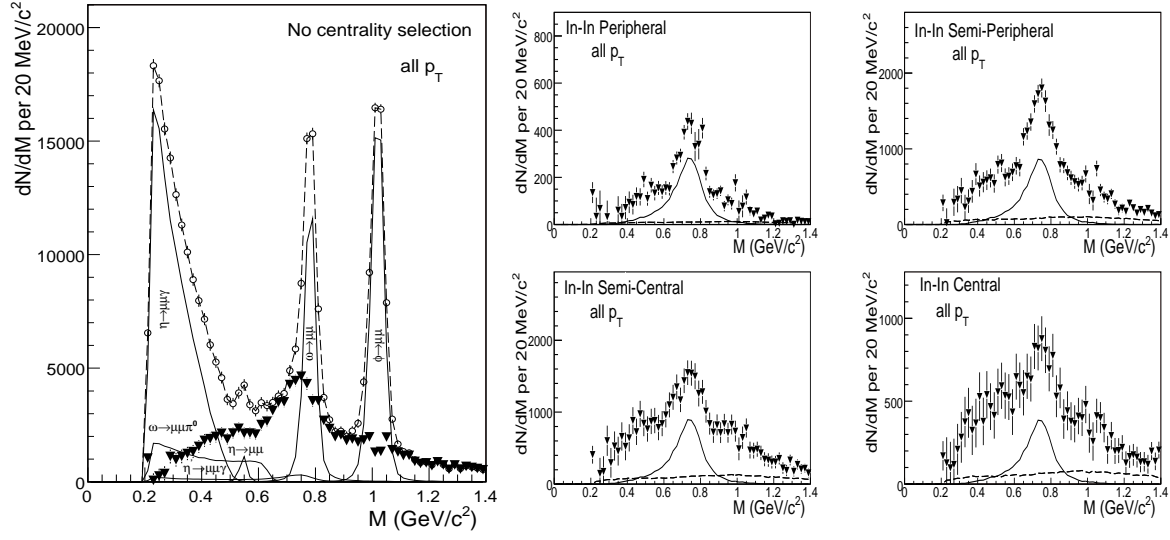
4

Figure 3: Left: isolation of an excess above the hadron decay cocktail. Total data (open circles), individual cocktail sources (solid), difference data (thick triangles), sum of cocktail sources and difference data (dashed). Right: excess mass spectra without p_T selection. The cocktail ρ (solid) and the level of uncorrelated charm decays (dashed) are shown for comparison.
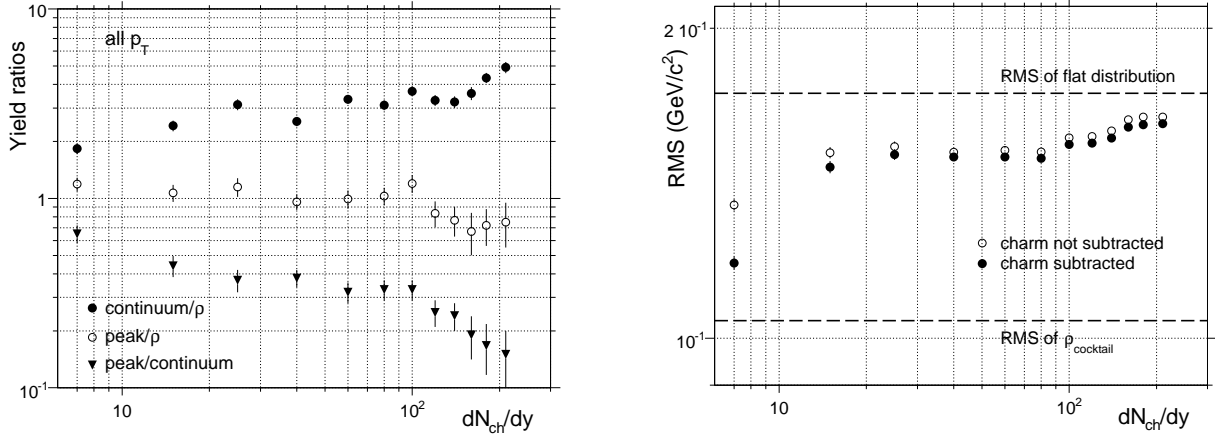

Figure 4: Left: Yield ratios continuum/ρ, peak/ρ, and peak/continuum. Right: RMS of the excess mass spectra in the window $0.44 < M < 1.04$ GeV/c^2

dominated by $\pi\pi$ annihilation. The theoretical description of the radiation via an intermediate ρ is composed of three elements: the photon propagator, a Boltzmann factor and the ρ spectral function. If no cuts on p_T are applied, the falling acceptance at low masses roughly compensates the steep rise due to the photon propagator

and the Boltzmann factor. Thus, within 20%, the excess spectra can be interpreted as spectral functions of the ρ, averaged over momenta and the complete space-time evolution of the fireball. The broad continuum-like part of the spectra may then reflect the early history close to the QCD boundary with a nearly divergent width, while the narrow peak on top may be due to the late part close to thermal freeze-out, approaching the nominal width.

The literature contains countless predictions for the change of the ρ properties in
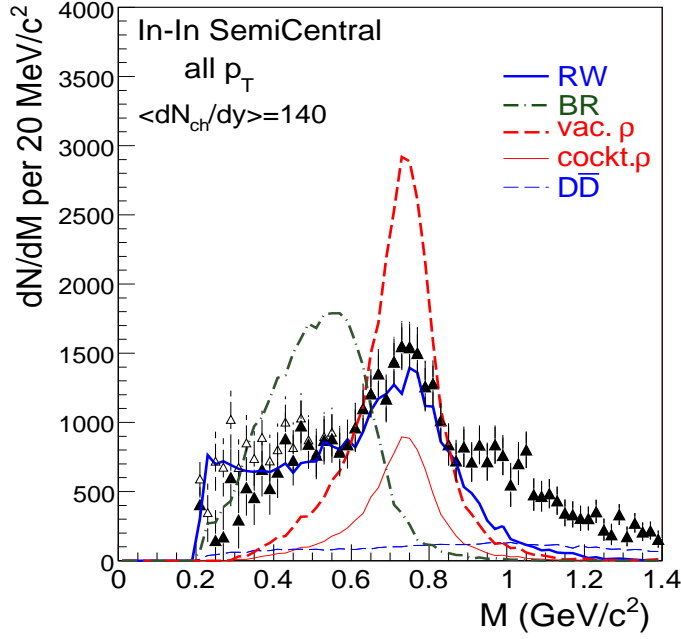

Figure 5: Comparison of excess mass spectrum with no p_T cut to model predictions made for In-In at $dN_{ch}/d\eta = 140$ (semicentral bin). Cocktail ρ (thin solid), unmodified ρ (dashed), in-medium broadening ρ [13, 14], in-medium moving ρ related to [15, 16] (dashed-dotted), uncorrelated charm (thin dashed). Errors are purely statistical. The open data point show the difference spectrum resulting from a decrease of the subtracted η yield by 10%.

hot and dense matter. To a large extent they all predict a strong broadening, while there is no consensus on what should happen to the pole mass. The predictions of the two main theoretical models which appeared in the past decade, the "broadening scenario" of Rapp/Wambach et al. [13, 14] and the "moving mass scenario" of Brown/Rho et al. [15, 16], could not be discriminated with the small CERES statistics in Pb-Au collisions. In fig. 5 these predictions are compared to the NA60 In-In data for the semi-central bin; the unmodified ρ is also shown. The theoretical spectra are independently normalized in the mass interval $M < 0.9$ GeV/c^2 in order to concentrate on the spectral shapes, independent of the uncertainties of the fireball

evolution. The unmodified ρ - either the cocktail ρ bound to the ratio $\rho/\omega = 1.2$ or the ρ produced in pion annihilation assuming no in-medium changes (the vacuum ρ) - is clearly ruled out. The moving mass scenario related to Brown/Rho scaling, which fit the CERES data [6, 7, 8], is also ruled-out. Only the broadening scenario appears to be in fair agreement with the data.

Further insight should come from the study of the p_T spectra [12]. First results of acceptance-corrected m_T spectra are shown in fig. 6. Again, remarkable and partially unexpected characteristics show up. The spectra (on the left panel) show a trend at small m_T opposite to what is expected from radial flow which predicts a flattening. In addition, a surprising mass dependence is visible, with the largest mass showing the steepest slope. The right panel shows the inverse slope parameter T_{eff} as obtained from differential fits to a sliding m_T window with the function $\exp(-m_T/T_{eff})$, where these tendencies appear even more clearly. No theoretical predictions, even the newest, are able to provide a satisfactory description of the data. We expect that these precise p_T dependencies will provide more insight into the different emission sources which seem to exist in different mass regions.
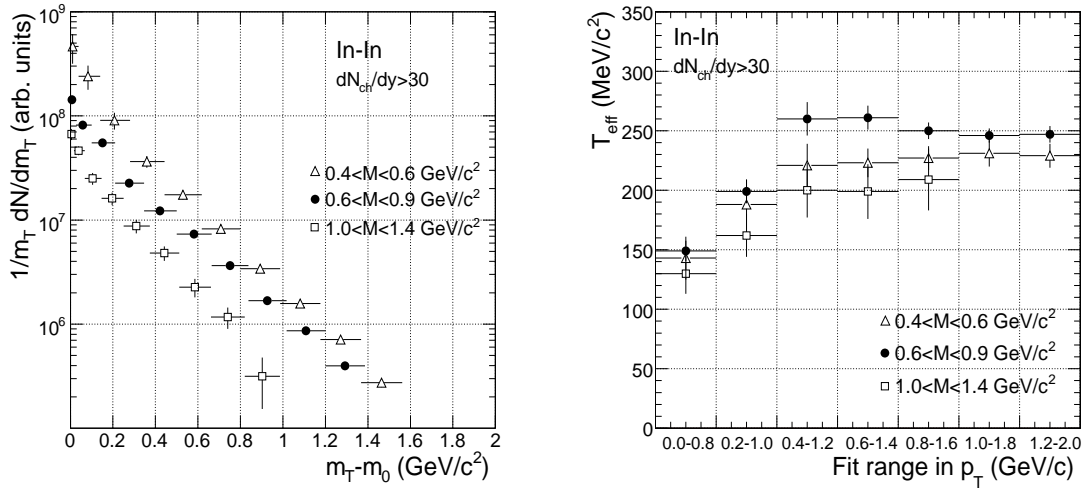

Figure 6: Left: acceptance corrected m_T spectra in different mass intervals integrated in centrality (with the exception of the peripheral bin). Right: Inverse slope T_{eff} parameter from differential fits of the m_T spectra (see text).

3 ϕ meson production

The study of ϕ production in heavy-ion collisions was originally motivated by the fact that it carries information about strangeness production. It has been argued that, close to the phase boundary, the spectral function of the ϕ, and thus its mass, width and branching ratios, could be modified [17]. Besides that, from the comparison of

the p_T distributions of the ϕ and other mesons, it is in principle possible to extract information about the average radial velocity (radial flow) and temperature of matter at kinetic freeze-out. Since these keep memory of the thermodynamic conditions present at earlier collision stages, their knowledge is quite useful to get insight into the fireball evolution. The study of radial flow is in progress, including also the p_T spectra of the ω meson and of the charged hadrons. Indirect information about radial flow, however, can already be obtained now from the study of the p_T spectrum of the ϕ meson alone.

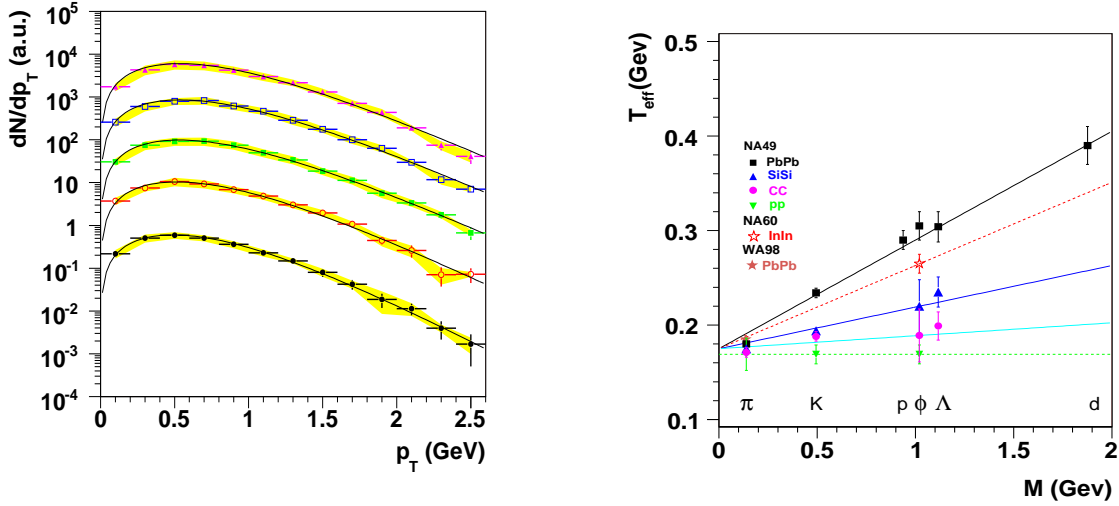NA60 has measured the p_T distribution of the ϕ in In-In collisions, with a broad p_T

Figure 7: Left: ϕ transverse momentum distributions in In-In as a function of centrality. From top to bottom: central to peripheral spectra. The bands show the systematic error. Right: T slope parameter as a function of particle mass for central events in several collision systems. The NA60 data point was obtained from a fit in the range $0 < p_T < 1.6$ GeV/c.

coverage ($0 < p_T < 3$ GeV/c) [18, 19]. Events in a narrow mass window centered at the ϕ pole ($0.98 < M < 1.06$ GeV/c^2) were selected from the mass distribution after combinatorial background subtraction. The p_T spectrum of the continuum below the ϕ was estimated and subtracted by selecting events in two side-windows in mass ($0.88 < M < 0.92$ GeV/c^2 and $1.12 < M < 1.16$ GeV/c^2), thus taking account also of the fake matches. The p_T spectra, corrected for acceptance and reconstruction efficiency, are shown in fig. 7 (left panel). For the moment, the data are fitted with the simple exponential function: $1/p_T \, dN/dp_T = C \cdot \exp\left(-m_T/T\right)$. The value of T for central collisions is compatible with the NA49 systematics versus mass for different collision systems, as shown in Fig. 7 (right panel).

Fig. 8 shows T as a function of the number of participants, obtained performing the fit on two different p_T windows. The first (left panel) is a low p_T window ($p_T < 1.6$
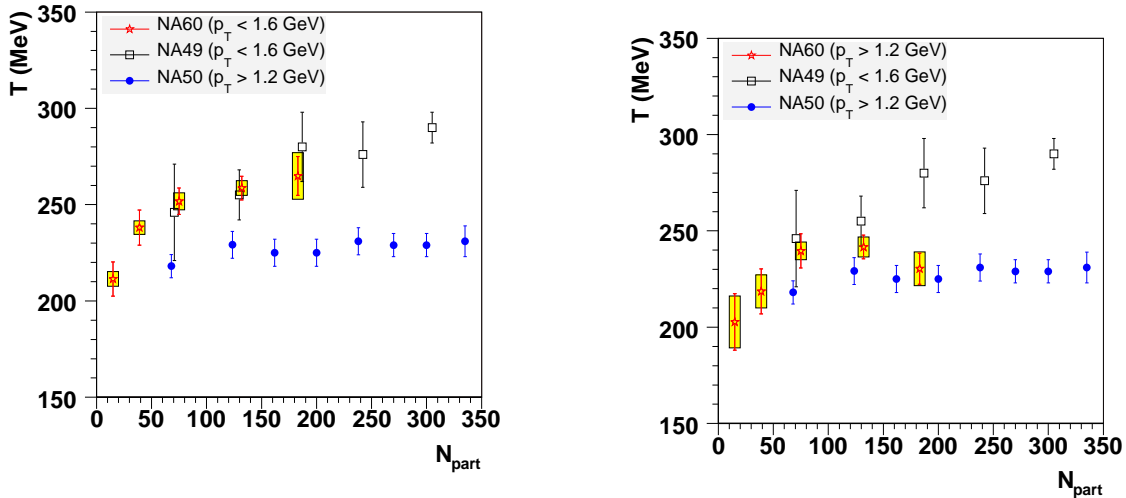
Figure 8: Left: T slope parameter as a function of number of participants (open red stars) and comparison to the T slope measured by NA49 (open black squares) and NA50 (full blue circles) in Pb-Pb collisions. Fit performed in the NA49 range $0 < p_T < 1.6$ GeV/c. Right: same as left, but fit performed in the NA50 range $1.2 < p_T < 2.6$ GeV/c.

GeV/c), chosen to overlap with the p_T region covered by the NA49 experiment. The second (right panel) is a a high p_T window ($p_T > 1.2$ GeV/c), chosen to overlap with the p_T region covered by the NA50 experiment.

The inverse slope parameter T is found to rise with centrality. This is a strong hint for the presence of radial flow, as the effective value of T is larger than the kinetic freeze-out temperature because of radial flow (which is expected to rise with centrality). A flattening of the centrality dependence for the fit in the high p_T range is again quite suggestive of the presence of radial flow.

The present results agree with those of the NA49 experiment [20] in the overlapping p_T region. The flattening at high p_T also goes in the direction of the NA50 points, though there is still some quantitative difference which does not seem to be entirely explained by the radial flow (though some care is needed because of the comparison of two different nuclear systems).

4 Prompt and open charm dimuons in the intermediate mass region

In the intermediate mass region ($1.2 < M < 2.7$ GeV/c^2) an excess over the Drell-Yan and $D\bar{D}$ sources was observed in S-U and Pb-Pb collisions by NA38/NA50 [22, 23] and in S-W collisions by HELIOS-3 [24]. To assess the exact nature of this excess,

9

either due to an increase of open charm production, or to thermal dimuons, requires separating the open charm contribution from the prompt dimuons.

In NA60 this is done by measuring the offset of the muons with respect to the interaction vertex, exploiting the long lifetime of D mesons: $c\tau = 312$ μm for D^+ and 123 μm for D^0. It is then fundamental to evaluate the precision in determining dimuon vertices; for that the dimuon decay of the J/ψ is used. At SPS energies there is no feed-down from beauty decays, and consequently all J/ψ mesons promptly decay at the interaction vertex. Thus, the dimuon vertexing resolution is determined from the "offset" of the J/ψ dimuon vertex with respect to the interaction vertex, evaluated using all reconstructed vertex tracks. The vertexing resolution depends in a critical way on the precision of the pixel telescope alignment. Originally, this was done by using calibration data taken when significant changes in the pixel set-up occurred. It was assumed that the alignment would not change for the data taken with the same setup.

Preliminary results from an analysis of the data based on this calibration, presented at the Quark Matter conference in 2005 [25], indicated that the observed excess was due to a prompt source. Later on, a much finer alignment procedure was developed based on the idea to process every run with the alignment algorithm such as to obtain custom alignment parameters for every few hours of beam time. This allowed in the present on-going analysis, as discussed in what follows, a much more robust determination of this extra yield of prompt dimuons with respect to the Drell-Yan yield [26]. Figure 9 shows the vertexing resolution before (left panel) and after (right panel) the fine alignment for both transverse coordinates: X (in the bending plane) and Y (in the non bending plane). Besides a large reduction of the width of these distributions (by some 30%), also the non-gaussian tails are not so prominent. As
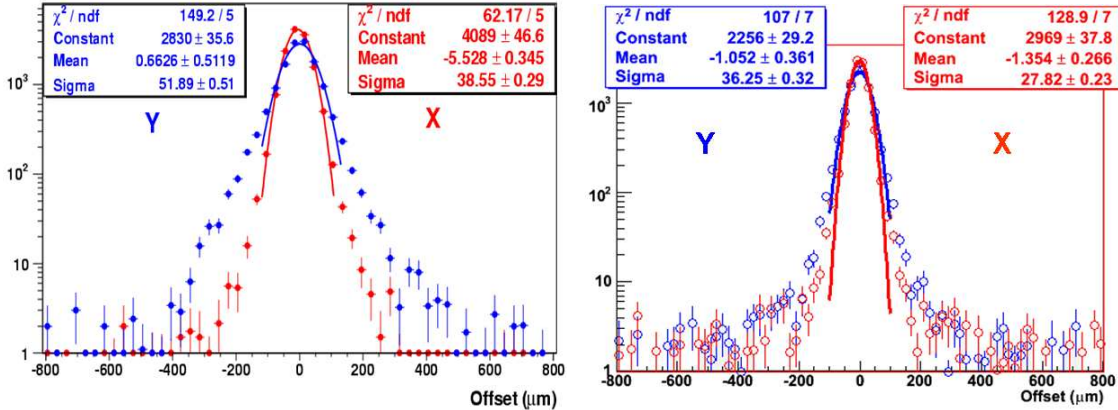

Figure 9: Left panel: distribution of the differences of the transverse coordinates of the J/ψ and interaction vertices, before (left). Right panel: after the fine alignment of the vertex tracker. An improvement of the resolution of about 30% can be deduced for both directions.

described in [25, 4], the vertexing precision also depends on the momentum of the

10

muons. Therefore, when evaluating whether a muon is far from the interaction vertex, the absolute values (in μm) cannot be used, and we have to use weighted offsets, dimensionless quantities which, provided all errors are properly estimated, behave as a reduced χ^2: $\Delta_\mu = \sqrt{\Delta x^2 V_{xx}^{-1} + \Delta y^2 V_{yy}^{-1} + 2\Delta x \Delta y V_{xy}^{-1}}$ for single muons and $\Delta = \Delta_{\mu\mu} = \sqrt{(\Delta_{\mu 1}^2 + \Delta_{\mu 2}^2)/2}$ for dimuons, where V^{-1} is the inverted error matrix from the vertex fit and the muon extrapolation. For J/ψ decays, the increase in quality of the weighted offsets is also remarkable, as depicted in Fig. 10. The tail of the distribution previously extending to large values is highly suppressed after the fine alignment. As mentioned above, the main goal of the present analysis is to assess the
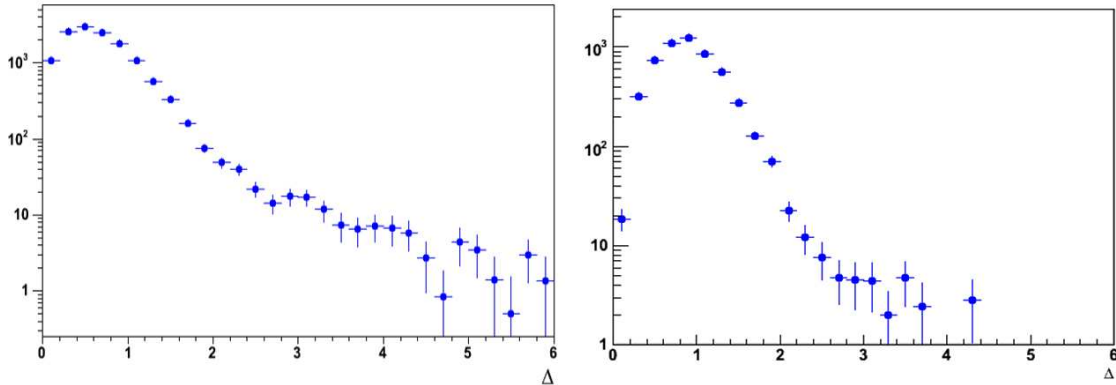

Figure 10: Weighted distance in the transverse plane between the J/ψ and interaction vertices before (left) and after (right) the fine alignment. It can be seen that the tail at high values vanishes and that the distribution now peaks at around unity, as expected.

yield of prompt dimuons compared to the expected Drell-Yan yield. Drell-Yan and open charm events decaying into two muons were generated with Pythia [27], using the CTEQ6L [28] set of parton distribution functions. First, the mass spectrum is fitted fixing the Drell-Yan contribution to be within the interval 0.9–1.1 of the yield expected from the measured high-mass dimuons, as described in [25, 4], and leaving the open charm contribution free. The fit, shown in Fig. 11 (left panel), reproduces the results seen by NA38 and NA50: the charm contribution fills the mass distribution with a reduced χ^2 of 1.8.

The analysis of the shape of the weighted offsets is the tool to assess in a quantitative way the nature of the excess. For the shape of the prompt contribution, a combination of the data under the J/ψ and ϕ peaks is used, whereas for open charm decays we need to use the one given by Monte Carlo. Nonetheless, for open charm decays the detector description in the Monte Carlo is properly done by smearing the offsets of single muons so that the measured distributions are very well reproduced. The smearing algorithm is tuned from the comparison between generated and measured J/ψ events and does not bias the analysis since each muon is treated individually [4]. After the fine alignment, the amount of smearing needed to bring the simulated
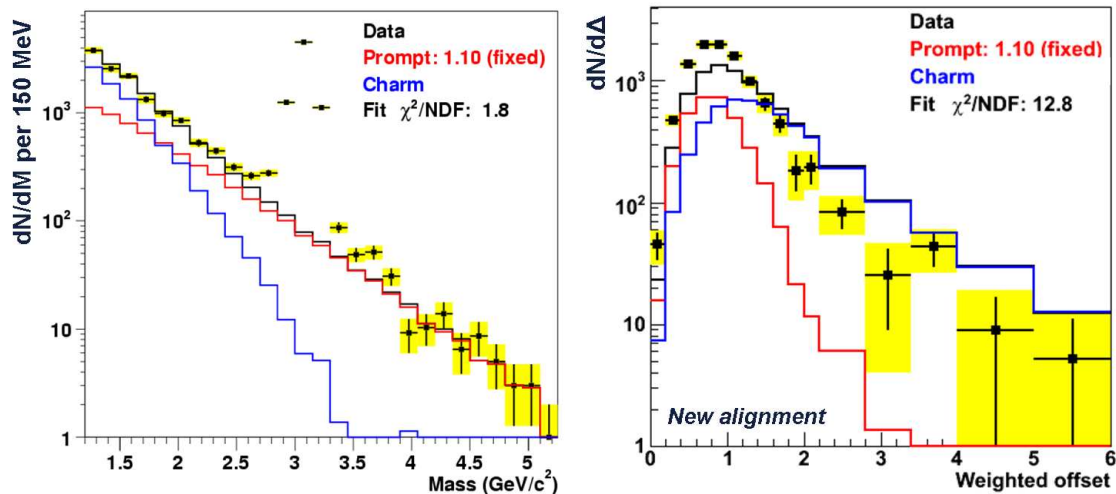
11

Figure 11: Left panel: Fit to the intermediate mass region fixing the Drell-Yan contribution from the high-mass region and letting the open charm contribution free. Right panel: The same normalisations clearly fail to describe the weighted offset data.

events to the same level of precision of the data is significantly smaller than previously.

First, the normalisations found in the fit to the mass spectrum (fig. 11, left panel) are imposed also to the analysis of the weighted offset distribution. As shown in fig. 11 (right panel), the charm contribution overshoots the data in the tail, whereas the prompt contribution largely undershoots the data at the peak (the reduced χ^2 is 13). In the next step the weighted offset distribution is fitted leaving free the normalisations of both the prompt and charm contributions. As shown in fig. 12, an extremely good agreement with the data is found (reduced $\chi^2 = 0.4$) if the yield of prompt dimuons is 2.65 ± 0.12 times larger than the expected Drell-Yan yield.

The offset analysis has thus uncovered a source of prompt dimuons which is roughly 1.6 times larger than the "conventional" Drell-Yan in the intermediate mass range. After having determined the nature and magnitude of the intermediate mass region excess, a characterisation of this prompt source of dimuons in terms of its transverse momentum and its centrality dependence is needed and presently under investigation.

5 J/ψ production

As suggested by Matsui and Satz in 1986 [29], J/ψ suppression is one of the most interesting signatures for the formation of a deconfined phase. The NA38 and NA50 experiments have extensively studied J/ψ production in different colliding systems, like p-A, S-U and Pb-Pb [30]. The pattern observed in Pb-Pb collisions indicates that below a certain centrality threshold the J/ψ production is well described by normal nuclear absorption; on the contrary, above this threshold, an anomalous suppression
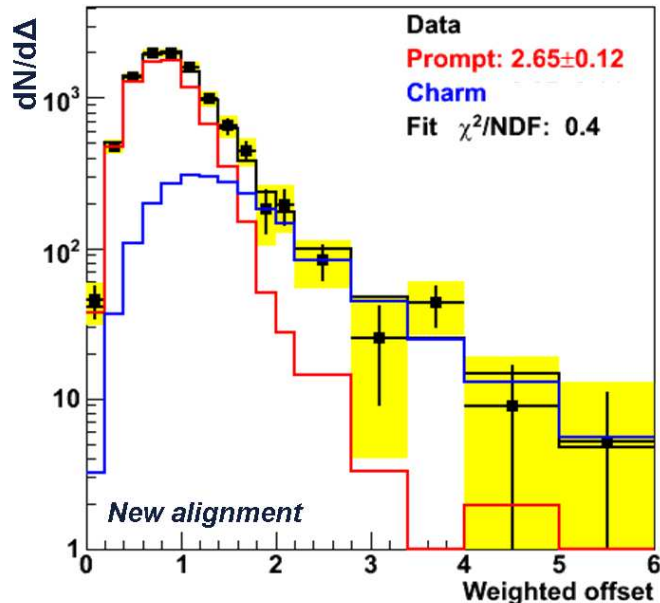
Figure 12: Description of the IMR weighted offset data as a superposition of open charm decays and prompt dimuons. The latter source is found to be 2.65 ± 0.12 times larger than the expected Drell-Yan yield.

sets in with a J/ψ yield considerably lower than expected from normal nuclear absorption.

NA60 has investigated if the suppression is already present in a system lighter than Pb-Pb. The comparison between different colliding systems should also allow to understand which is the physics variable at the origin of the J/ψ suppression.

In principle, the use of matched muons is helpful also for the J/ψ analysis, since requiring that the dimuon vertex coincides with the most upstream interaction, we reject J/ψ events not produced in a primary In-In collision. In addition, the J/ψ mass resolution improves from ~ 105 MeV to ~ 70 MeV, and the combinatorial background under the J/ψ reduces from ~ 3 % to $\sim 1\%$. However, the reduction of the available statistics due to the matching efficiency can be an important drawback as shown below. In addition, as shown in fig. 13 (left panel), the J/ψ peak is clearly visible on top of the underlying continuum even without matching, which is then not strictly needed for this analysis. Therefore matching is required only if it does not represent a major limitation to the accuracy of the results. If no matching is required, a cut based on the distance between the beam axis and the extrapolated muon tracks at the target position has to be applied, in order to select dimuons produced in the target region.

Collisions occurring outside the target region are rejected, thanks to the good z vertex resolution of ~ 200 μm. To extract the J/ψ yield we select dimuons in the phase space window $0 < y_{cms} < 1$ and $-0.5 < \cos\theta_{CS} < 0.5$, where θ_{CS} is the polar decay angle of the muons in the Collins-Soper reference frame.
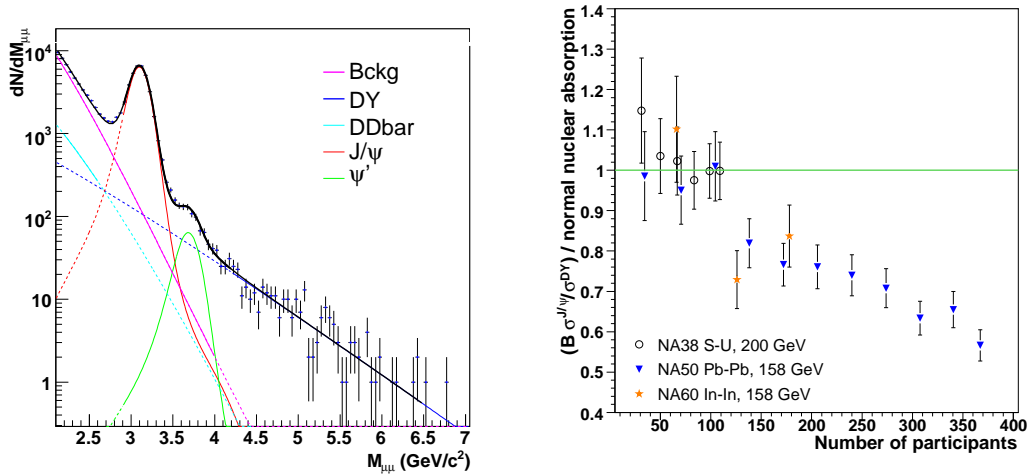
13

Figure 13: Left panel: dimuon invariant mass (corresponding to the muon spectrometer 6500 A setup). Right panel: $J/\psi\,/\,\mathrm{DY}$ analysis compared to the normal nuclear absorption curve vs. the number of participants, compared with the NA50 and NA38 results.

The first analysis performed is similar to the one of NA38/50. It makes use of the ratio of J/ψ to Drell-Yan (DY) cross sections [31, 32], the latter scaling with the number of nucleon-nucleon collisions. This approach, although robust by itself, suffers from the low number of high-mass Drell-Yan events. For that reason the matching, which would further reduce the statistics without increasing the robustness of the results, is not required. After the event selection, we are left with $\sim$45000 J/ψ and $\sim$320 Drell-Yan events, with mass above $4.2\ \mathrm{GeV}/c^2$. The ratio between J/ψ and DY is extracted by fitting the opposite-sign dimuon mass spectrum with a superposition of the open charm, J/ψ and DY processes, as shown in fig. 13 (left panel). Results obtained from the two sets of data corresponding to the two configurations of the muon spectrometer are found to be statistically compatible and, therefore, are averaged.

While the study of the J/ψ to DY cross sections ratio is free from systematic errors, the statistical error is large, and for that reason the $J/\psi\,/\,\mathrm{DY}$ ratio cannot be studied in more than three centrality bins. The reference pattern, if nuclear absorption is the only suppression mechanism, is obtained within the Glauber model, assuming that the J/ψ is a hard process and using σ_{abs}=4.18 $\pm$ 0.35 mb as nuclear absorption cross section of the $c\bar{c}$, as measured by NA50 [30]. Fig. 13 (right panel) shows the $J/\psi\,/\,\mathrm{DY}$ results divided by the corresponding reference ratio and plotted as a function of the number of participants. This centrality estimator is directly obtained from the ZDC energy E_{ZDC} using the Glauber model and taking into account the detector resolution.

Comparing to the NA38 and NA50 results, we can conclude that an anomalous suppression of the J/ψ is present already in In-In collisions. However the small number

14

of bins prevents an accurate study of the J/ψ centrality dependence.

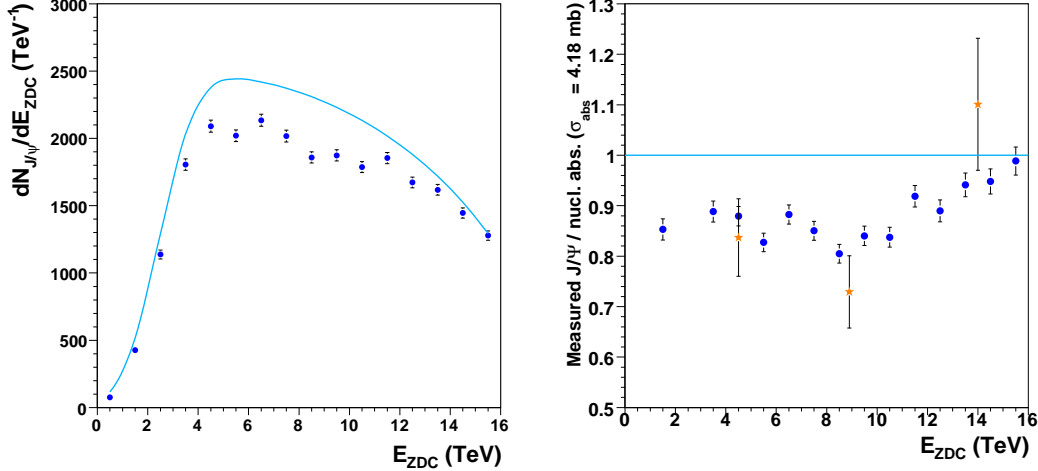In order to overcome the problem of the low Drell-Yan statistics, we studied di-

Figure 14: Left panel: Measured J/ψ compared to the normal nuclear absorption curve vs. E_{ZDC}. Right panel: ratio between measured J/ψ and the absorption curve (stars: standard analysis). The three most central bins have been grouped together to reduce statistical fluctuations.

rectly the J/ψ centrality distribution as a function of E_{ZDC}[31, 32]. In this case the matching of the muon tracks is required, because a more accurate selection of the J/ψ events is needed to reduce possible systematic effects. In this analysis ~ 29000 J/ψ events are left after the subtraction of the small amount of combinatorial background. Since the number of J/ψ is not normalized to other data collected under the same conditions, small inefficiencies due to the event selection and to the reconstruction procedure do not cancel out and the centrality distribution of J/ψ events has to be corrected for them. Reinteraction of Indium fragments in the target region is also considered. Since this analysis is affected by negligible statistical errors ($< 2\%$), an accurate evaluation of the systematic errors has been performed. The estimated systematic error amounts to $\sim 10\%$ independent of centrality, except for the most central bin ($E_{ZDC} < 3$ TeV), where it is more sizable. This implies that the shape of the suppression pattern is determined with good precision, while the absolute normalization is more uncertain.

The J/ψ centrality distribution is compared to the expected pattern assuming nuclear absorption as the only suppression source. In this analysis the relative normalization between data and reference curve is not fixed a priori; we normalize the result imposing that the ratio between data and absorption curve, integrated over centrality, is the same as in the standard $J/\psi/\mathrm{DY}$ analysis, i.e. 0.87 ± 0.05. Therefore, the 6% statistical error on the $J/\psi/\mathrm{DY}$ analysis results in an overall factor, independent on the centrality, affecting the normalization of the direct J/ψ analysis. Results are shown in fig. 14 (left panel) as a function of the energy released in the ZDC. In fig. 14

15

(right panel) the ratio between the measured and the expected yield is shown.
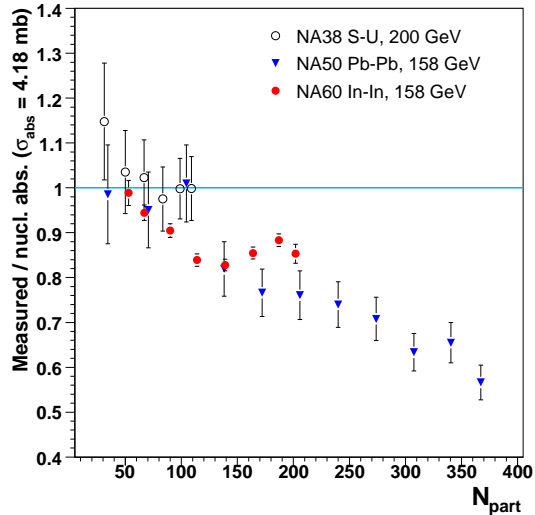   This analysis confirms a departure from the expected normal nuclear absorption,

Figure 15: Ratio between measured J/ψ and the absorption curve as a function of N_{part} for S-U, Pb-Pb and In-In collisions.

already roughly observed in the standard $J/\psi\,/\,DY$ analysis at ~ 12 TeV (corresponding to $N_{part} \sim 82$), followed by a flatter behaviour for more central events.
In fig. 15 the In-In results, rebinned to reduce the remaining statistical fluctuations, are shown together with the previous results of NA38/NA50 as a function of the number of participant nucleons. Although this comparison must be considered as preliminary, due to possible systematics related to the use of different centrality estimators (transverse energy for NA38/NA50, E_{ZDC} for NA60), a fair agreement between the various systems can be seen.

6   Elliptic flow of charged hadrons and of J/ψ

In non-central heavy-ion collisions, the overlap region of the two colliding nuclei is not azimuthally symmetric. The rescattering between the produced particles can transfer this spatial asymmetry to an asymmetry in the momentum space. The study of such an anisotropy in the momentum space allows to get insight in the early stage of the fireball expansion (e.g. on the thermalization of the system, which is a key element for the formation of the QGP).
The anisotropy shows up as characteristic azimuthal correlations between particle momenta and the reaction plane. This is the plane defined by the beam direction $\vec{z}$ and the impact parameter vector $\vec{b}$. To quantify the anisotropic flow, the coefficients of a Fourier expansion of the azimuthal distributions with respect to the reaction plane are evaluated [33]. The reaction plane is experimentally not directly accessible,

16

but it can be determined using the anisotropic flow itself, independently for each harmonic n of the anisotropic flow. A detailed overview on several methods is given in [34]. The method we employ is the so-called event plane method [34], relating the azimuthal emission angles ϕ_i of all the charged particles i to the azimuthal angle Ψ of the event plane (an estimate of the reaction plane). The event plane angle is corrected for the highly asymmetric acceptance of the NA60 experiment in the azimuthal angle ϕ by applying a recentering [35] and a flattening procedure [34]. We can correlate
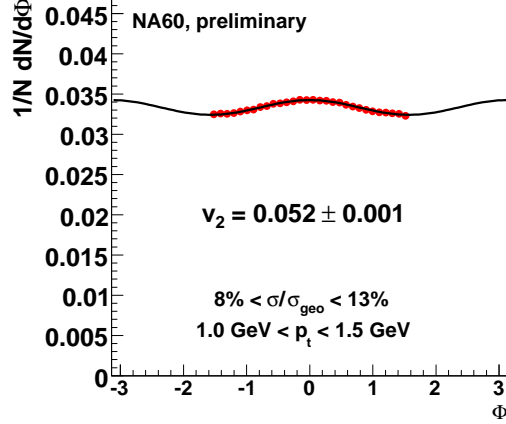

Figure 16: Azimuthal emission pattern of charged particles in In+In at 158 AGeV. The line represents a fit to the data (see text).

the emission angles ϕ_{lab} of single particles with this event plane angle Ψ considering the azimuthal emission patterns $\mathrm{d}N/\mathrm{d}\phi$, with $\phi = \phi_{\mathrm{lab}} - \Psi$. This is shown in fig. 16. Since the directed flow, meaning the first harmonic ($n = 1$), is zero at midrapidity due to symmetry reasons we concentrate on the second harmonic ($n = 2$) only. The distribution is fitted with the function $1 + 2v_2' \cos(2\phi)$, where $v_2' = \langle \cos(2 \cdot \phi) \rangle$. This coefficient has to be corrected for the event plane resolution to obtain the real elliptic flow coefficient $v_2 = v_2'/\langle \cos[2 \cdot \Delta\Psi] \rangle$. To determine the correction factors, the data have been divided into subevents and the method described in [36] has been applied.

The resulting elliptic flow coefficients v_2 for all charged particles are displayed as a function of p_T in fig. 17 (left panel). Since non-flow correlations due to the HBT affect the results at low p_T, the results are shown for $p_T > 0.5$ GeV/c only. The flow coefficients rise with p_T and show a saturation at higher momenta as already previously observed in Pb+Pb collisions at the SPS [37] as well as at higher energies at RHIC [38]. The elliptic flow has been also studied as a function of centrality using the energy deposited in the ZDC. Fig. 17 (right panel) shows v_2 for charged particles as a function of p_T for four centrality bins. The quoted fractions of the total geometrical cross section have been calculated within the Glauber model.
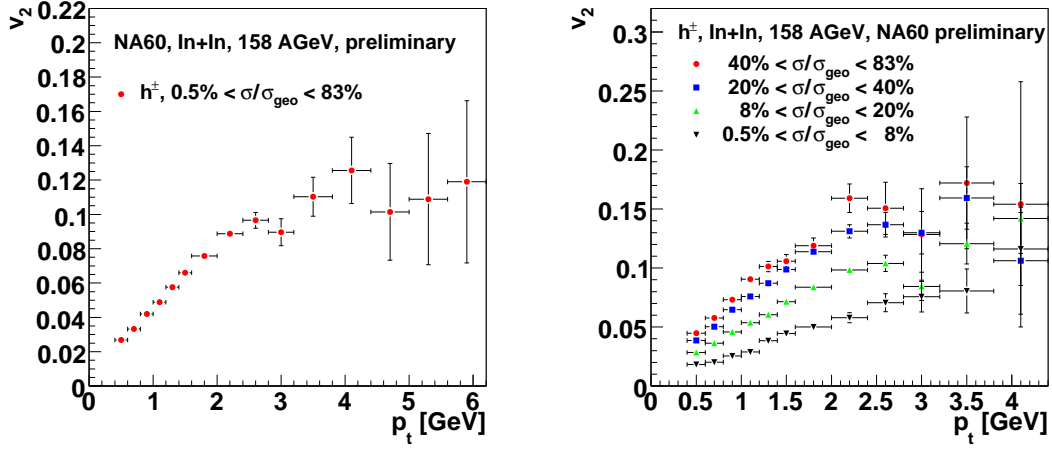
17

Figure 17: Left: the elliptic flow coefficient v_2 of charged hadrons as a function of p_T. Right: the elliptic flow coefficient v_2 of charged hadrons as a function of p_T for various collision centralities.
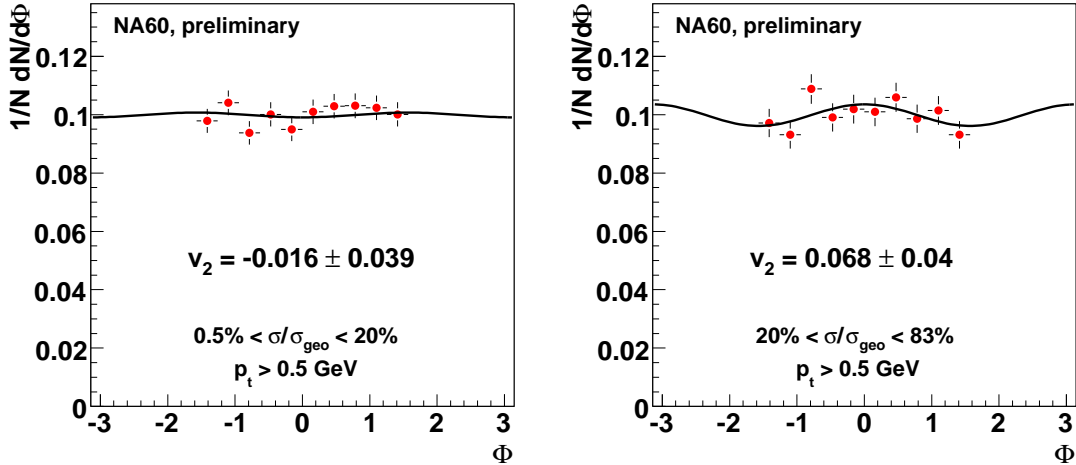
Figure 18: Azimuthal emission patterns of J/ψ in In+In at 158 AGeV, on the left hand side for more central collisions, on the right hand side for more peripheral collisions.

Having determined the orientation of the reaction plane with the charged particle tracks measured in the vertex tracker we can then determine the azimuthal angle emission pattern of the J/ψ with respect to this plane as well. Fig. 18 shows the azimuthal angle distributions for the J/ψ, on the left hand side for central events

18

$(0.5\% < \sigma/\sigma_{\mathrm{geo}} < 20\%)$, on the right hand side for peripheral events $(20\% < \sigma/\sigma_{\mathrm{geo}} < 83\%)$. In total these distributions contain approximately 12000 J/ψ events, which correspond to about 50% of the full statistics available for this type of analysis. The peripheral data seem to indicate a non-isotropic emission pattern but the limited statistics does not allow to draw a solid conclusion for the moment. The analysis of the remaining statistics is under way.

7 Outlook of the proton data analysis

As mentioned in the introduction, the p-A data collected during the 2004 run consist of two parts, both collected with the same system of Al, Be, Cu, In, W, Pb and U subtargets. Four days were devoted to collect data with a 158 GeV/c beam using the vertex tracker made of 13 ALICE pixel planes, 2 ATLAS pixel planes and 2 BNL microstrip planes. These data were collected with the specific goal to measure the the nuclear dependence of the J/ψ absorption cross section at the same energy as the In-In data. This will allow to avoid to rely on measurements performed at different energy, which has been a source of systematic uncertainty so far.

In the remaining data taking period, a 400 GeV/c beam was used with a few different setups of the vertex tracker including also ATLAS microstrip planes. The collected data will allow to perform several measurements, as (i) the determination of the nuclear dependence of the χ_c absorption cross section, whose importance stems from the fact that a significant fraction of J/ψ comes from the decays of the χ_c, (ii) the measurement of the open charm yield in pA in order to provide a baseline for the In-In data, and (iii) detailed studies of the ρ line shape, $\rho - \omega$ interference and the ω Dalitz decay form factor, which are not yet precisely known in pp and pA interactions; these could be also of some help to reduce systematic uncertainties in the In-In data analysis.

The total collected statistics corresponds to ~ 30000 J/ψ reconstructed in the muon spectrometer (before matching to the tracks in the vertex tracker) for the 158 GeV/c sample, and ~ 10 times more for the 400 GeV/c sample.

Since 4 MWPC planes (out of 24) in the muon spectrometer broke during the data taking period, we had to modify the reconstruction code and settings in order to bring the reconstruction efficiency to its usual rate at the expense of a negligible increase of the background level.

 The reconstruction of charged particle tracks in the vertex tracker and their matching to muons required much more effort than expected. As we learned from our experience with the In-In 2003 data (see also the section on the intermediate mass region), it is not enough to align the tracker planes with special runs (with the vertex dipole magnet switched off) taken after each change of the detector setup. In order to account for the minute changes in the geometry of the setup, we had to perform a run-by-run realignment of the preliminary reconstructed data with the semi-automatic program used for the In-In 2003 sample. For example, in order to keep the residuals
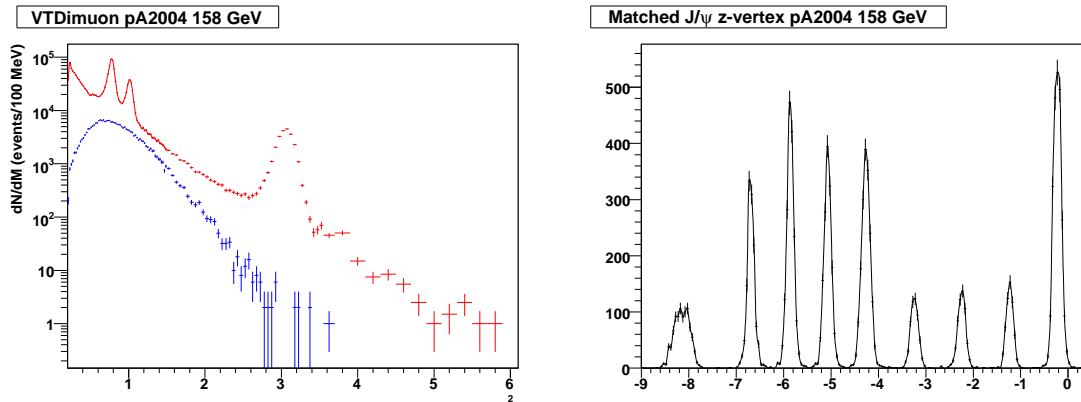
Figure 19: Left panel: Matched dimuon invariant mass (like sign pairs in blue and opposite sign pairs in red) for the 158 GeV/c data. Right panel: distribution of dimuon vertices of the 158 GeV/c data.

at the level below a few microns, we had to define 75 different setups for the 124 runs of the 158 GeV/c data. At this moment, the alignment of the 158 GeV/c data is completed, while for the runs taken with the 400 GeV/c beam only setups without the ATLAS microstrips have been aligned. The preprocessing of the remaining data will require additional efforts for the calibration of the microstrips and it is presently in progress.

Currently all the data collected with the 158 GeV/c beam are reconstructed, and the tracks in the vertex region are matched to muons in the spectrometer. This provided ~ 11000 matched J/ψ dimuons, in good agreement with expectations. Fig. 19 (left panel) shows the mass spectrum for matched dimuons, while the distribution of the dimuon vertices is shown in the right panel of fig. 19. As one can see, the dimuons originating from different targets are very well separated. The analysis of the J/ψ production cross section and its nuclear dependence is under way, and we hope to present preliminary results at the Quark Matter 2006 conference. Concerning the reconstruction of the 400 GeV/c data, we are currently performing the final checks of the alignment quality for the runs not using the ATLAS strips and plan to start the final reconstruction within a short time from now.

Now that the In-In data analysis is entering in a mature phase, several teams will focus more deeply also in the analysis of the pA data. We expect to have the first physics results for the beginning of next year.

References

[1] G. Usai et al. (NA60) Eur. Phys. J. **C43**, 415 (2005)

[2] M. Keil et al., Nucl. Instr. Meth. **A539**, 137 (2005) and **A546**, 448 (2005)

[3] R. Shahoyan et al. (NA60), Eur. Phys. J. **C43**, 209 (2005)

[4] A. David (2006), CERN-THESIS-2006-007

[5] R.D. Pisarski, Phys. Lett. **110B**, 155 (1982)

[6] G. Agakichiev et al. (CERES), Eur. Phys. J. **C4**, 231 (1998)

[7] G. Agakichiev et al. (CERES), Phys. Rev. Lett. **75**, 1272 (1995)

[8] G. Agakichiev et al. (CERES), Phys. Lett. **B422**, 405 (1998); B. Lenkeit et al., Nucl. Phys. **A661**, 23c (1999); G. Agakichiev et al. (CERES), Eur. Phys. J. **C41**, 475 (2005)

[9] R. Arnaldi et al. (NA60), Phys. Rev. Lett. **96** (2006) 162302

[10] S. Damjanovich et. al (NA60), Nucl. Phys. **A774**, 715 (2006)

[11] S. Damjanovich et. al (NA60), Hot Quarks 2006 proc., to be published in Eur. Phys. J. C (2006)

[12] S. Damjanovich et. al (NA60), Hard Probes conf. proc., to be published in Nucl. Phys. A (2006)

[13] G. Chanfray, R. Rapp, J. Wambach, Phys. Rev. Lett. **76**, 368 (1996); R. Rapp, G. Chanfray, J. Wambach, Nucl. Phys. **A617**, 472 (1997)

[14] R. Rapp, J. Wambach, Adv. Nucl. Phys. **25**, 1 (2000)

[15] G.E. Brown, M. Rho, Phys. Rev. Lett. **66**, 2720 (1991); G.Q. Li, C.M. Ko, G.E. Brown, Phys. Rev. Lett. **75** 4007 (1995)

[16] G.E. Brown, M. Rho, Phys. Rept. **363**, 85 (2002)

[17] E.V. Shuryak., Nucl. Phys. **A661**, 119 (1999)

[18] A. de Falco et al. (NA60), Nucl. Phys. **A774**, 719 (2006)

[19] M. Floris et al. (NA60), Hot Quarks 2006 proc., to be published in Eur. Phys. J. C (2006)

[20] S. V. Afanasev et al. (NA49), Phys. Lett. **B491**, 59 (2000)

[21] B. Alessandro et al. (NA50), Phys. Lett. **B555**, 147 (2003)

[22] C. Lourenco et al., Nucl. Phys. **A566**, 77c (1994)

[23] M.C. Abreu et al., Eur. Phys. J. **C14**, 443 (2000)

[24] A.L.S. Angelis et al., Eur. Phys. J. **C13**, 433 (2000)

[25] R. Shahoyan et al., Nucl. Phys. **A774**,677 (2006)

[26] A. David et al., Hard Probes conf. proc., to be published in Nucl. Phys. A (2006)

[27] T. Sjostrand, L. Lonnblad, S. Mrenna, Pythia 6.2: Physics and manual.

[28] J. Pumplin et al., JHEP **07**, 12 (2002)

[29] T. Matsui, H. Satz, Phys. Lett. **B178**, 416 (1986)

[30] M. Abreu et al. (NA50), Eur. Phys. J. **C39**, 335 (2005)

[31] R. Arnaldi et al. (NA60), Nucl. Phys. **A774**, 711 (2006)

[32] R. Arnaldi et al. (NA60), Hard Probes conf. proc., to be published in Nucl. Phys. A (2006)

[33] A. Forster et al. (NA60), Strangeness in Quark Matter conf. proc., to be published in J. Phys. G (2006)

[34] A.M. Poskanzer, S.A. Voloshin, Phys. Rev. **C58** 1671 (1998)

[35] C. Alt et al. (NA49), Phys. Rev. **C68** 034903 (2003)

[36] J. Y. Ollitrault, nucl-ex/97110003

[37] J. Milošević et al. (NA45), SQM2006 proceedings

[38] M. Oldenburg et al. (STAR), Quark Matter 2005, Nucl. Phys. **A** in print, nucl-ex/0510026; S. Adler et al. (PHENIX), Phys. Rev. Lett. **91** 182301 (2003)

NA60 Publications 2004 − 2006

Physics papers

1. R. Arnaldi *et al.*, NA60 Collaboration,
   Dimuon production in p nucleus and nucleus nucleus collisions: The NA60 experiment,
   To appear in the proceedings of 39th Rencontres de Moriond on QCD and High-Energy Hadronic Interactions, arXiv:hep-ex/0406054.

2. P. Sonderegger for the NA60 Collaboration,
   Accurate measurements of dimuon production in the NA60 experiment,
   J. Phys. G **30** (2004) S1027.

3. A. Colla for the NA60 Collaboration,
   Study of the J/ψ Production and Suppression in In-In Collisions at the CERN SPS,
   J. Phys. G **31** (2005) S317.

4. M. Floris *et al.* [NA60 Collaboration],
   Charged particle multiplicity measurements in NA60,
   J. Phys. Conf. Ser. **5** (2005) 55.

5. R. Shahoyan *et al.* [NA60 Collaboration],
   Study of dimuon production in Indium-Indium collisions with the NA60 experiment,
   To appear in the proceedings of 40th Rencontres de Moriond on QCD and High Energy Hadronic Interactions, La Thuile, Aosta Valley, Italy, 12-19 Mar 2005, arXiv: hep-ex/0505049

6. J. Lozano *et al.*, NA60 Collaboration,
   Dimuon Production in Proton-Nucleus and Heavy-Ion Collisions with the NA60 Detector at the CERN SPS,
   to appear in the Proceedings of the International Nuclear Physics Conference (INPC 2004), Göteborg.

7. A. De Falco *et al.*, NA60 Collaboration,
   First results of the NA60 experiment at the CERN SPS,
   to appear in the Proceedings of the NPDC18 Conference 2004, Prag.

8. E. Scomparin [NA60 Collaboration],
   Dilepton and charmonium production at the SPS,
   Prepared for 32nd International Conference on High-Energy Physics (ICHEP 04), Beijing, China, 16-22 Aug 2004, Published in *Beijing 2004, ICHEP, vol. 1* 385-388

9. H. Ohnishi *et al.*, NA60 Collaboration,
   J/ψ Production in Indium-Indium Collisions, The NA60 Experiment,
   J. Phys. G **31** (2005) S1209.

10. S. Damjanovic for the NA60 Collaboration,
    *First results from NA60 on low mass muon pair production in In-In collisions
    at 158 GeV/nucleon*,
    J. Phys. G **31** (2005) S903.

11. K. Borer *et al.* for the NA60 Collaboration,
    First results of the NA60 experiment at the CERN SPS,
    Nucl. Phys. A **749** (2005) 251.

12. R. Arnaldi *et al.* for the NA60 Collaboration,
    J/ψ production in Indium-Indium collisions,
    Eur. Phys. J. C **43** (2005) 161.

13. R. Shahoyan *et al.* for the NA60 Collaboration,
    A first look at open charm production in Indium-Indium collisions at SPS energies,
    Eur. Phys. J. C **43** (2005) 209.

14. G. Usai *et al.* for the NA60 Collaboration,
    Low Mass Dimuon Production in Indium-Indium Collisions at SPS energies,
    Eur. Phys. J. C **43** (2005) 415.

15. H.K. Woeheri *et al.* for the NA60 Collaboration,
    Low mass dimuon production in proton-nucleus collisions with the NA60 apparatus,
    Eur. Phys. J. C **43** (2005) 407.

16. S. Damjanovic *et al.* for the NA60 Collaboration,
    First measurement of the ρ spectral function in high-energy nuclear collisions
    Quark Matter 2005 (QM05), Budapest, Hungary,
    Nucl. Phys. A **774** (2006) 715

17. A. De Falco *et al.* for the NA60 Collaboration,
    φ production in p-A and In-In collisions
    Quark Matter 2005 (QM05), Budapest, Hungary,
    Nucl. Phys. A **774** (2006) 719

18. R. Shahoyan *et al.* for the NA60 Collaboration,
    Charm and intermediate mass dimuons in Indium-Indium collisions
    Quark Matter 2005 (QM05), Budapest, Hungary,
    Nucl. Phys. A **774** (2006) 677

19. R. Arnaldi *et al.* for the NA60 Collaboration,
    Anomalous J/ψ suppression in In-In collisions at 158 GeV/nucleon
    Quark Matter 2005 (QM05), Budapest, Hungary,
    Nucl. Phys. A **774** (2006) 711

20. E. Scomparin *et al.* for the NA60 Collaboration,
    Dimuon and charm production in In-In collisions at the CERN SPS
    Quark Matter 2005 (QM05), Budapest, Hungary,
    Nucl. Phys. A **774** (2006) 67

21. G. Usai *et al.* for the NA60 Collaboration,
    Results from the NA60 experiment at the CERN SPS
    PANIC 2005, Santa Fe, USA,
    AIP conf. proc. in press.

22. C. Lourenco *et al.* [NA60 Collaboration],
    J/psi suppression in indium-indium collisions at SPS energies,
    PoS **HEP2005** (2006) 133.

23. H. K. Woehri *et al.* [NA60 Collaboration],
    Low mass dimuon production in proton-nucleus and indium-indium collisions,
    PoS **HEP2005** (2006) 132.

24. R. Shahoian *et al.* [NA60 Collaboration],
    Intermediate mass dimuon production in indium-indium collisions at the CERN SPS
    PoS **HEP2005** (2006) 131.

25. P. Pilot *et al.* for the NA60 Collaboration,
    J/ψ production in Indium-Indium collisions at SPS energies
    AIP Conf. Proc. **806** (2006) 279.

26. M. Floris *et al.*, for the NA60 Collaboration,
    phi production in proton nucleus and indium indium collisions at the CERN
    AIP Conf. Proc. **828** (2006) 309.

27. A. Förster for the NA60 Collaboration,
    Latest results from NA60,
    International Conference on Strangeness in Quark Matter, UCLA, Los Angeles,
    to be published in J. Phys. G (2006).

28. R. Arnaldi *et* al. [NA60 Collaboration],
    First Measurement of the ρ Spectral Function in High-Energy Nuclear Collisions,
    Phys. Rev. Lett. **96** (2006) 162302.

25

29. M. Floris *et al.*, for the NA60 Collaboration,
    Phi production in NA60
    to be published in Eur. Phys. J. C (2006)

30. S. Damjanovic *et al.* for the NA60 Collaboration,
    First Measurement of the ρ Spectral Function in Nuclear Collisions,
    to be published in Eur. Phys. J. C (2006)

31. S. Damjanovic *et al.* for the NA60 Collaboration,
    NA60 results on the ρ spectral function in indium-indium collisions,
    2nd International Conference on Hard and Electromagnetic Hard Probes 2006,
    Asilomar Conference Grounds, Pacific Grove, California, June 9-16, 2006
    to be published in Nucl. Phys. A (2006)

32. A. David *et al.* for the NA60 Collaboration,
    Charm and intermediate mass dimuons in NA60 ,
    2nd International Conference on Hard and Electromagnetic Probes of High-Energy Nuclear Collisions, Asilomar Conference Grounds, Pacific Grove, California, June 9-16, 2006; to be published in Nucl. Phys. A (2006)

33. R. Arnaldi *et al.* for the NA60 Collaboration,
    J/psi production in In-In and p-A collisions in NA60 ,
    2nd International Conference on Hard and Electromagnetic Probes of High-Energy Nuclear Collisions, Asilomar Conference Grounds, Pacific Grove, California, June 9-16, 2006; to be published in Nucl. Phys. A (2006)

Instrumental papers

34. A. David for the NA60 Collaboration,
    Pioneering instrumentation aspects of NA60,
    J. Phys. G **30** (2004) S1101.

35. M. Floris et al.
    The NA60 experiment readout architecture,
    IEEE Trans. Nucl. Sci, 51 (2004) 430.

36. M. Floris et al.
    A new PCI card for readout in high energy physics experiments,
    IEEE Trans. Nucl. Sci, 51 (2004) 2086.

37. K. Banicz *et al.*,
    Operation and performance of the NA60 silicon pixel telescope,
    CERN-PH-EP-2004-021, Nucl. Instrum. Meth.   A **539** (2005) 137.

38. K. Banicz *et al.*,
    The NA60 Silicon Vertex Spectrometer,
    Nucl. Instrum. Meth. A **546**, 51 (2005).

39. M. Keil *et al.*,
    Studies of radiation effects in the NA60 silicon pixel detectors,,
    Nucl. Instrum. Meth. A **546** (2005) 448.

40. M. Keil *et al.*,
    The NA60 silicon pixel telescope,
    Nucl. Instrum. Meth. A **549** (2005) 20.

41. M. Keil *et al.*,
    Radiation damage effects in the NA60 silicon pixel detectors,
    Nucl. Instrum. Meth. A **552** (2005) 239.

42. A. David *et al.*
    The silicon vertex telescope of the NA60 experiment,
    PoS **HEP2005** (2006) 379.

43. J. M. Heuser *et al.*,
    Experience with the NA60 silicon pixel vertex tracker in a harsh radiation environment,
    Nucl. Instrum. Meth. A **560** (2006) 9.

44. M. Floris *et al.*,
    The silicon pixel detector of the NA60 experiment,
    Nucl. Phys. Proc. Suppl. **150** (2006) 231.